Electronic Absorption and MCD Spectra for $Pd(AuPPh_3)_8^{2+}$, $Pt(AuPPh_3)_8^{2+}$, and Related Platinum-Centered Gold Cluster Complexes

Michael J. Adrowski and W. Roy Mason*

Department of Chemistry, Northern Illinois University, DeKalb, Illinois 60115-2862

Received June 14, 1996[⊗]

Electronic absorption and 7.0 T magnetic circular dichroism (MCD) spectra in the UV−vis region, 1.6 to ~4.0 μm^{-1} ($1\ \mu m^{-1} = 10^4\ cm^{-1}$) are reported for $[Pd(AuPPh_3)_8](NO_3)_2$ and $[Pt(AuPPh_3)_8](NO_3)_2$ in acetonitrile solutions at room temperature. The MCD spectra are better resolved than the absorption spectra and consist of both *A* and *B* terms. The spectra are interpreted in terms of D_{4d} skeletal geometry and MO's that are approximated by 5s and 6s orbitals for Pd and Pt/Au atoms, respectively. The lowest energy excited configurations and states are attributed to intraframework (IF) Au_8^{2+} transitions. Evidence is also presented for Pt 5d → Au 6s transitions in the MCD spectra for $Pt(AuPPh_3)_8^{2+}$. Acetonitrile solution absorption and MCD spectra for the related Pt-centered cluster complexes $[Pt(CO)(AuPPh_3)_8](NO_3)_2$, $[Pt(AuP(p\text{-tolyl})_3)_8](NO_3)_2$, $[Pt(CuCl)(AuPPh_3)_8](NO_3)_2$, $[Pt(AgNO_3)(AuPPh_3)_8](NO_3)_2$, $[Pt(Hg)_2(AuPPh_3)_8](NO_3)_2$, $[Pt(HgCl)_2(AuPPh_3)_8](BF_4)_2$, and $[Pt(HgNO_3)_2(AuPPh_3)_8](BF_4)_2$ are also reported and interpreted within the context of the model developed for the $M(AuPPh_3)_8^{2+}$ complexes.

Introduction

In recent years, several heteronuclear gold cluster complexes of the general formula $M(AuPAr_3)_n^{m+}$ have been prepared and investigated.[1,2] These complexes have interesting structures and properties. For example, $[Pd(AuPPh_3)_8](NO_3)_2$, $PdAu_8^{2+}$, and $[Pt(AuPPh_3)_8](NO_3)_2$, $PtAu_8^{2+}$, in the solid state, have a structure which consists of a centered crown (approximately D_{4d} skeletal symmetry), **1**.[3,4] The Au−Au distances range from 2.77 to 2.86

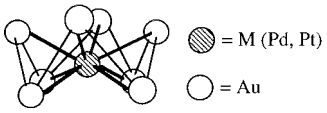

1

Å and are shorter than in metallic gold (2.886 Å). The average Pd− or Pt−Au distances are 2.62 and 2.64 Å, respectively. The centered crown structure is also exhibited by $[Au(AuP(p\text{-}C_6H_4OMe)_3)_8](NO_3)_3$,[5] but the analogous gold-centered cluster with PPh_3 ligands $[Au(AuPPh_3)_8](NO_3)_3$, Au_9^{3+}, exhibits a different structure with a D_{2h} symmetry, which may be viewed as a centered icosahedral fragment, **2**.[6]

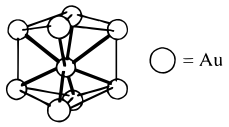

2

Among the more interesting chemical properties of the $PdAu_8^{2+}$ and $PtAu_8^{2+}$ clusters is their ability to function as homogeneous and heterogeneous catalysts for H_2/D_2 exchange.[7,8] Also, the $PtAu_8^{2+}$ cluster complex reacts irreversibly with CO and CNR (R = *i*-Pr, *t*-Bu), while $PdAu_8^{2+}$ reacts reversibly only with CO, and Au_9^{3+} is much less reactive and does not react appreciably with either CO or CNR.[9]

In spite of the interesting structures and properties of these cluster complexes, very little is known about their electronic structure. Some extended Hückel MO calculations for the $PtAu_8^{2+}$ and $[Pt(CO)(AuPPh_3)_8](NO_3)_2$, $Pt(CO)Au_8^{2+}$, cluster complexes have been presented recently, but low-energy excited states were not identified.[10] Also some preliminary electronic spectral data for the strongly colored $PdAu_8^{2+}$ and $PtAu_8^{2+}$ ions and some other related gold cluster complexes have been reported,[1,8,11] but these spectra have not been assigned and the associated excited states remain largely uncharacterized.

In order to provide insight into the electronic structure and interpret the electronic spectra of these and other heteronuclear bimetallic cluster complexes, a systematic investigation of representative complexes by means of magnetic circular dichroism (MCD) spectroscopy has been initiated. An MCD study of Au_9^{3+} and the related $Au_8(PPh_3)_8^{2+}$ complex from this laboratory was reported earlier.[12a,b] In the present paper, the absorption and MCD spectra for the $PdAu_8^{2+}$ and $PtAu_8^{2+}$ ions in acetonitrile solutions are reported and interpreted and comparisons are made with the earlier spectra for Au_9^{3+}. The absorption and MCD spectra for several other structurally related

[⊗] Abstract published in *Advance ACS Abstracts,* March 1, 1997.

(1) Pignolet, L. H.; Aubart, M. A.; Craighead, K. L.; Gould, R. A. T.; Krogstad, D. A.; Wiley, J. S. *Coord. Chem. Rev.* **1995**, *143*, 219.
(2) (a) Mingos, D. M. P.; Watson, M. J. *Adv. Inorg. Chem.* **1992**, *39*, 327 and references therein. (b) Steggerda, J. J. *Comments Inorg. Chem.* **1990**, *11*, 113.
(3) Ito, L. N.; Johnson, B. J.; Mueting, A. M.; Pignolet, L. H. *Inorg. Chem.* **1989**, *28*, 2026.
(4) (a) Bour, J. J.; Kanters, R. P. F.; Schlebos, P. P. J.; Bosman, W. P.; Behm, H.; Beurskens, P. T.; Steggerda, J. J. *Recl. Trav. Chim. Pays-Bas* **1987**, *106*, 157. (b) Bour, J. J.; Kanters, R. P. F.; Schlebos, P. P. J.; Steggerda, J. J. *Recl. Trav. Chim. Pays-Bas* **1988**, *107*, 211.
(5) Briant, C. E.; Hall, K. P.; Mingos, D. M. P. *J. Chem. Soc., Chem. Commun.* **1984**, 290.
(6) Hall, K. P.; Mingos, D. M. P. *Prog. Inorg. Chem.* **1984**, *32*, 237 and references therein.
(7) Aubart, M. A.; Pignolet, L. H. *J. Am. Chem. Soc.* **1992**, *114*, 7901.
(8) Kappen, T. G. M. M.; Bour, J. J.; Schlebos, P. P. J.; Roelofsen, A. M.; van der Linden, J. G. M.; Steggerda, J. J.; Aubart, M. A.; Krogstad, D. A.; Schoondergang, M.F. J.; Pignolet, L. H. *Inorg. Chem.* **1993**, *32*, 1074.
(9) (a) Kanters, R. P. F.; Schlebos, P. P. J.; Bour, J. J.; Bosman, W. P.; Behm, H. J.; Steggerda, J. J. *Inorg. Chem.* **1988**, *27*, 4034. (b) Ito, L. N.; Felicissimo, A. M. P.; Pignolet, L. H. *Inorg. Chem.* **1991**, *30*, 988.
(10) Kanters, R. P. F.; Schlebos, P. P. J.; Bour, J. J.; Wijnhoven, J.; van der Berg, E.; Steggerda, J. J. *J. Organomet. Chem.* **1990**, *388*, 233.
(11) Schoondergang, M. F. J. Ph.D. Thesis, University of Nijmegen, 1992.
(12) (a) Jaw, H.-R. C.; Mason, W. R. *Inorg. Chem.* **1991**, *30*, 275. (b) Jaw, H.-R. C.; Mason, W. R. *Inorg. Chem.* **1991**, *30*, 3552.

S0020-1669(96)00699-4 CCC: $14.00

platinum-centered gold clusters were also measured in acetonitrile solution and are reported and interpreted herein. These complexes, which may be visualized as derivatives of $PtAu_8^{2+}$, include $[Pt(CO)(AuPPh_3)_8](NO_3)_2$, $[Pt(AuP(p\text{-tolyl})_3)_8](NO_3)_2$, $[Pt(CuCl)(AuPPh_3)_8](NO_3)_2$ (abbreviated $Pt(CuCl)Au_8^{2+}$), $[Pt(AgNO_3)(AuPPh_3)_8](NO_3)_2$ ($Pt(AgNO_3)Au_8^{2+}$), $[Pt(Hg)_2(AuPPh_3)_8](NO_3)_2$ ($Pt(Hg)_2Au_8^{2+}$), $[Pt(HgCl)_2(AuPPh_3)_8](BF_4)_2$ ($Pt(HgCl)_2Au_8^{2+}$), and $[Pt(HgNO_3)_2(AuPPh_3)_8](BF_4)_2$ ($Pt(HgNO_3)_2Au_8^{2+}$).

Experimental Section

Preparation of Compounds. $[Pd(AuPPh_3)_8](NO_3)_2$. The purple octakis((triphenylphosphine)gold)palladium(2+) nitrate, $[Pd(AuPPh_3)_8](NO_3)_2$, was prepared according to the literature method.[3] A CH_2Cl_2 solution of $Pd(PPh_3)_4$ and $Au(PPh_3)NO_3$ was treated with a methanol solution of $NaBH_4$ (mole ratio 1:8:5.6 for the three reactants, respectively) under N_2. The solid was then crystallized from methanol/diethyl ether. The compound gave satisfactory elemental analysis, and the ^{31}P NMR [$\delta(CDCl_3) = 51.8$ ppm (s)] and UV−vis spectra compared favorably with published data.[1,3,11]

$[Pt(AuPPh_3)_8](NO_3)_2$. The brown octakis((triphenylphosphine)gold)platinum(2+) nitrate, $[Pt(AuPPh_3)_8](NO_3)_2$, was also prepared according to the literature[4] from $[Pt(H)(PPh_3)(AuPPh_3)_7](NO_3)_2$, $Pt(H)Au_7^{2+}$, which was prepared by bubbling H_2 for 2 h through a THF solution of $Pt(PPh_3)_3$ and $Au(PPh_3)NO_3$ (1:6 molar ratio).[13] The $Pt(H)Au_7^{2+}$ starting material in CH_2Cl_2 was then treated with $Au(PPh_3)NO_3$ (1:2.2 molar ratio), along with a few drops of triethylamine. The solid obtained from the evaporation of the solvent was reprecipitated from 1:10 (v/v) methanol/diethyl ether. The compound gave satisfactory elemental analysis, and the UV−vis spectra and the ^{31}P NMR spectra [$\delta(CD_3OD) = 58.7$ (s with satellites; $^2J(^{195}Pt-^{31}P) = 493$ Hz); $\delta(CDCl_3) = 58.1$ (s with satellites; $^2J(^{195}Pt-^{31}P) = 497$ Hz)] compared favorably with published data.[1,4,8,10,11]

$[Pt(CO)(AuPPh_3)_8](NO_3)_2$. The bright red carbonyloctakis((triphenylphosphine)gold)platinum(2+) nitrate, $[Pt(CO)(AuPPh_3)_8](NO_3)_2$, was prepared according to the literature[9] by bubbling CO through an acetone solution of $[Pt(AuPPh_3)_8](NO_3)_2$ until dry. The solid gave satisfactory elemental analysis, and the UV−vis spectra and ^{31}P NMR spectra [$Pt(CO)Au_8^{2+}$ $\delta(CDCl_3) = 54.2$ (s with satellites), $^2J(^{195}Pt-^{31}P) = 391$ Hz] compared favorably with the published data.[1,9,11]

Other Cluster Complexes. The dark brown nitratosilver(I) octakis((triphenylphosphine)gold)platinum(2+) nitrate, $[Pt(AgNO_3)(AuPPh_3)_8](NO_3)_2$,[14] the dark brown chlorocopper(I) octakis((triphenylphosphine)gold)platinum(2+) nitrate, $[Pt(CuCl)(AuPPh_3)_8](NO_3)_2$,[11,15] the dark brown octakis((tri-*p*-tolylphosphine)gold)platinum(2+) nitrate, $[Pt(AuP(p\text{-tolyl})_3)_8](NO_3)_2$, the orange dimercury(0) octakis((triphenylphosphine)gold)platinum(2+) nitrate, $[Pt(Hg)_2(AuPPh_3)_8](NO_3)_2$,[16] the brown bis(chloromercury(I)) octakis((triphenylphosphine)gold)platinum(2+) tetrafluoroborate, $[Pt(HgCl)_2(AuPPh_3)_8](BF_4)_2$,[16,17] and the red brown bis(nitratomercury(I)) octakis((triphenylphosphine)gold)platinum(2+) tetrafluoroborate, $[Pt(HgNO_3)_2(AuPPh_3)_8](BF_4)_2$,[16] were all generously donated by Professor L. Pignolet. The silver and copper cluster complexes gave the following ^{31}P NMR spectra (δ in ppm). $Pt(AgNO_3)Au_8^{2+}$: $\delta(CD_3COCD_3) = 59.3$ (s with satellites), $^2J(^{195}Pt-^{31}P) = 497$ Hz; 60.8 (m, broad). $Pt(CuCl)Au_8^{2+}$: $\delta(CD_3COCD_3) = 59.3$ (s with satellites), $^2J(^{195}Pt-^{31}P) = 498$ Hz; 60.0 (m). The ^{31}P NMR for $Pt(AuP(p\text{-tolyl})_3)_8^{2+}$ gave $\delta(CD_3COCD_3) = 57.2$ (s with satellites), $^2J(^{195}Pt-^{31}P) = 497$ Hz. The dimercury cluster complexes gave ^{31}P NMR spectra that compared favorably with the published data:[1,16] $Pt(Hg)_2Au_8^{2+}$, $\delta(CD_3COCD_3) = 55.5$ (s with satellites), $^2J(^{195}Pt-^{31}P) = 486$ Hz, $^3J(^{199}Hg-^{31}P) =$ ca. 365 Hz and ca. 250 Hz; $Pt(HgCl)_2Au_8^{2+}$, $\delta(CD_3CN) = 61.5$ (s with satellites), $^2J(^{195}Pt-^{31}P) = 394$ Hz, $^3J(^{199}Hg-^{31}P) = 354$ Hz.

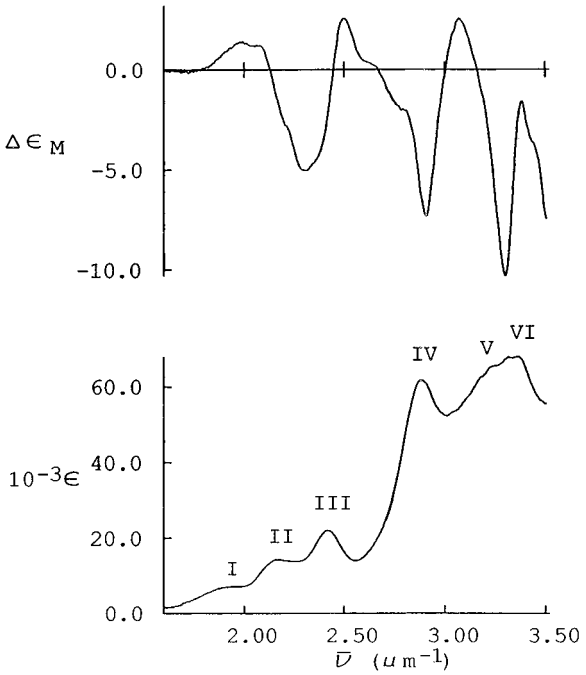

Figure 1. Magnetic circular dichroism (upper curve) and electronic absorption (lower curve) spectra for $[Pd(AuPPh_3)_8](NO_3)_2$ in acetonitrile at room temperature. $\Delta\epsilon_M$ has units of $(M\ cm\ T)^{-1}$, and ϵ has units of $(M\ cm)^{-1}$; $1\ \mu m^{-1} = 10^4\ cm^{-1}$.

Spectral Measurements. Preliminary electronic absorption spectra were measured for acetonitrile solutions of the cluster complexes by means of a Cary 1501 spectrophotometer. Absorption and MCD spectra were then recorded simultaneously and synchronously along the same light path by means of a spectrometer described previously.[18] A magnetic field of 7.0 T was obtained from a superconducting magnet system (Oxford Instruments SM2-7, fitted with a room-temperature bore tube). Spectral grade acetonitrile was used throughout, and all spectra were corrected for a solvent blank. Spectral measurements were limited to energies below ~4.0 μm^{-1} ($1\ \mu m^{-1} = 10^4\ cm^{-1}$) because of the onset of strong absorptions from the ligand phenyl substituents and the nitrate counterions. Absorption and MCD spectra obeyed Beer's law to within experimental error in the concentration range 10^{-4}-10^{-5} M. The solutions were not appreciably light sensitive and did not exhibit any noticeable changes during the time required to make spectral measurements (typically, 1 h per scan).

Results and Discussion

Electronic Absorption and MCD Spectra. Figures 1 and 2 show the electronic absorption and MCD spectra for $PdAu_8^{2+}$ and $PtAu_8^{2+}$, respectively, in acetonitrile at room temperature. Spectra for the Pt-centered cluster complexes $Pt(CO)Au_8^{2+}$, $Pt(CuCl)Au_8^{2+}$, $Pt(Hg)_2Au_8^{2+}$, and $Pt(HgCl)_2Au_8^{2+}$ are presented in Figures 3−6. The spectra for $Pt(AuP(p\text{-tolyl})_3)_8^{2+}$ and $Pt(AgNO_3)Au_8^{2+}$ are of similar quality and are very similar in pattern to the spectra for $PtAu_8^{2+}$. The spectra for $Pt(HgNO_3)_2Au_8^{2+}$ are very similar to the spectra for $Pt(HgCl)_2Au_8^{2+}$. Quantitative spectral data for all the cluster complexes are

(13) Kanters, R. P. F.; Bour, J. J.; Schlebos, P. P. J.; Bosman, W. P.; Behm, H.; Steggerda, J. J.; Ito, L. N.; Pignolet, L. H. *Inorg. Chem.* **1989**, *28*, 2591.
(14) (a) Kanters, R. P. F.; Schlebos, P. P. J.; Bour, J. J.; Bosman, W. P.; Smits, J. M. M.; Beurskens, P. T.; Steggerda, J. J. *Inorg. Chem.* **1990**, *29*, 324. (b) Kanters, R. P. F.; Bour, J. J.; Schlebos, P. P. J.; Steggerda, J. J. *J. Chem. Soc., Chem. Commun.* **1988**, 1634.
(15) Schoondergang, M. F. J.; Bour, J. J.; Schlebos, P. P. J.; Vermeer, A. W. P.; Bosman, W. P.; Smits, J. M. M.; Beurskens, P. T.; Steggerda, J. J. I*norg. Chem.* **1991**, *30*, 4704.
(16) Gould, R. A. T.; Craighead, K. L.; Wiley, J. S.; Pignolet, L. H. *Inorg. Chem*. **1995**, *34*, 2902.
(17) Bour, J. J.; Berg, V. D.; Schlebos, P. P. J.; Kanters, R. P. F.; Schoondergang, M. F. J.; Bosman, W. P.; Smits, J. M. M.; Beurskens, P. T.; Steggerda, J. J. *Inorg. Chem.* **1990**, *29*, 2971.
(18) Mason, W. R. *Anal. Chem.* **1982**, *54*, 646. The spectrometer has been upgraded by replacing the analog lock-in amplifier with a newer DSP Lock-in (Stanford Research Systems SR850) and by replacing the PDP 11/03 computer by a faster PDP 11/73 computer. The optical components and measurement methodology remain essentially the same.

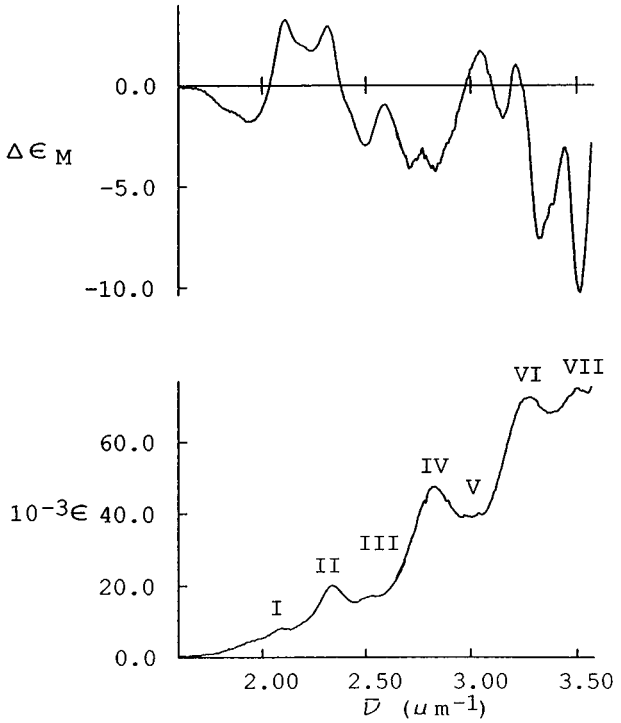

Figure 2. Magnetic circular dichroism (upper curve) and electronic absorption (lower curve) spectra for $[Pt(AuPPh_3)_8](NO_3)_2$ in acetonitrile at room temperature. The units are as in Figure 1.

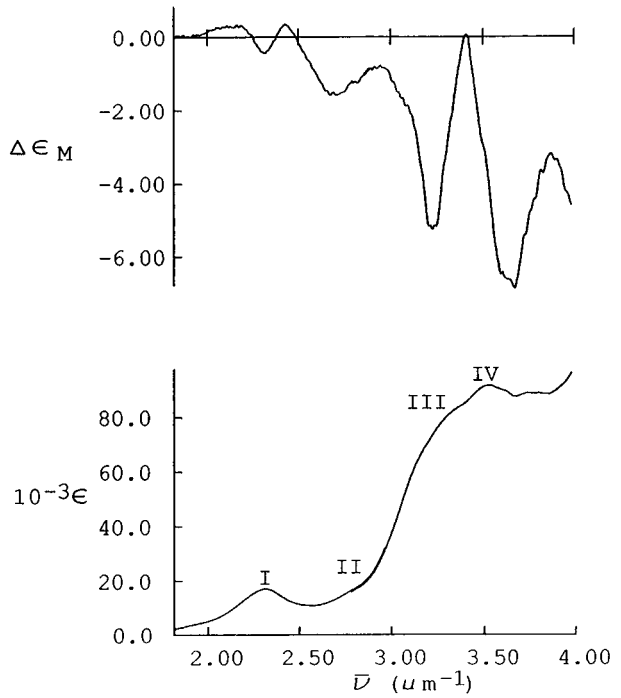

Figure 3. Magnetic circular dichroism (upper curve) and electronic absorption (lower curve) spectra for $[Pt(CO)AuPPh_3)_8](NO_3)_2$ in acetonitrile at room temperature. The units are as in Figure 1.

collected in Table 1 ($1\ \mu m^{-1} = 10^4\ cm^{-1}$). It may be noted that better resolution and more individual features are seen in the MCD spectra than in the absorption spectra. For example, the MCD spectra in Figures 1 and 2 show weak negative features at 1.69 μm^{-1} for $PdAu_8^{2+}$ and 1.84 and 1.95 μm^{-1} for $PtAu_8^{2+}$, in both cases, to lower energy than of the lowest energy absorption band maximum, band I. These MCD features must correspond to transitions unresolved in the absorption spectra. Underlying transitions are also indicated in the MCD spectra

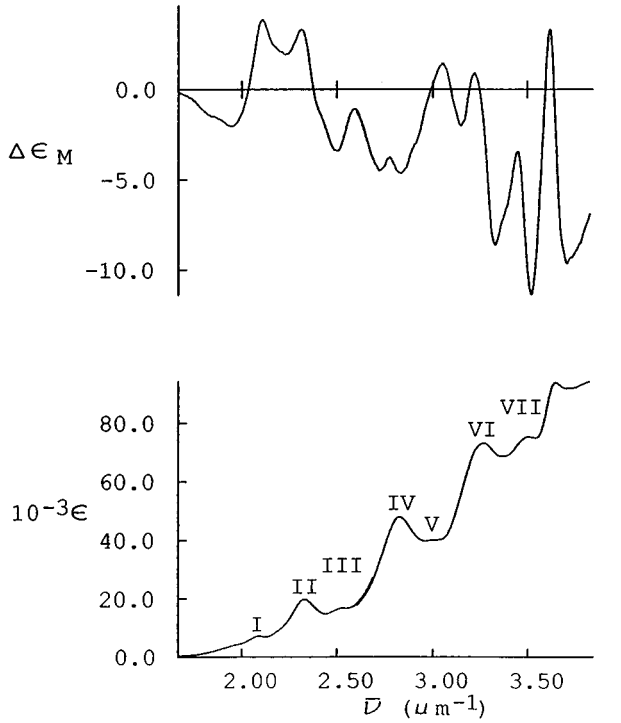

Figure 4. Magnetic circular dichroism (upper curve) and electronic absorption (lower curve) spectra for $[Pt(CuCl)(AuPPh_3)_8](NO_3)_2$ in acetonitrile at room temperature. The units are as in Figure 1.

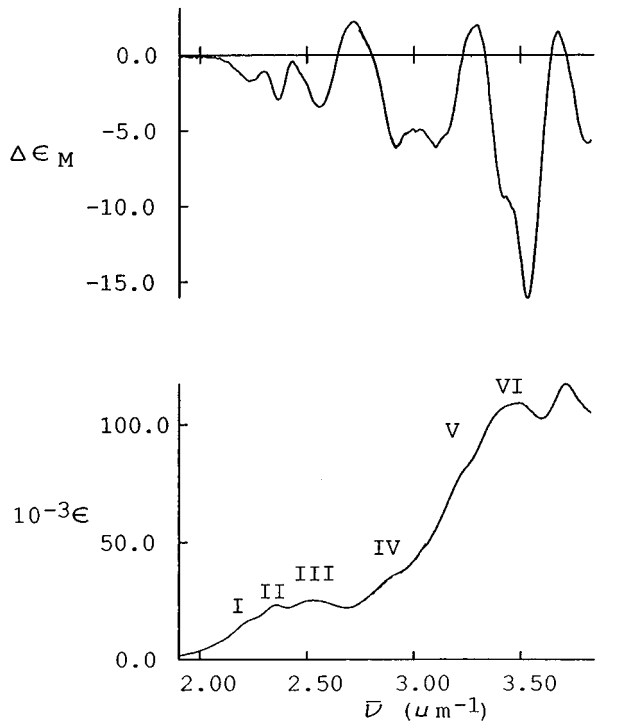

Figure 5. Magnetic circular dichroism (upper curve) and electronic absorption (lower curve) spectra for $[Pt(Hg)_2(AuPPh_3)_8](NO_3)_2$ in acetonitrile at room temperature. The units are as in Figure 1.

at 2.80 μm^{-1} and at 2.71 μm^{-1} between bands III and IV for $PdAu_8^{2+}$ and for $PtAu_8^{2+}$, respectively. The triphenylphosphine ligands and nitrate ions are transparent below $\sim$3.5 μm^{-1}. Therefore, bands below this energy for the cluster complexes are attributed to the intramolecular transitions within the metal cluster framework. Spectral features above $\sim$3.6 μm^{-1} were not investigated due to the strong ligand and counterion absorptions.

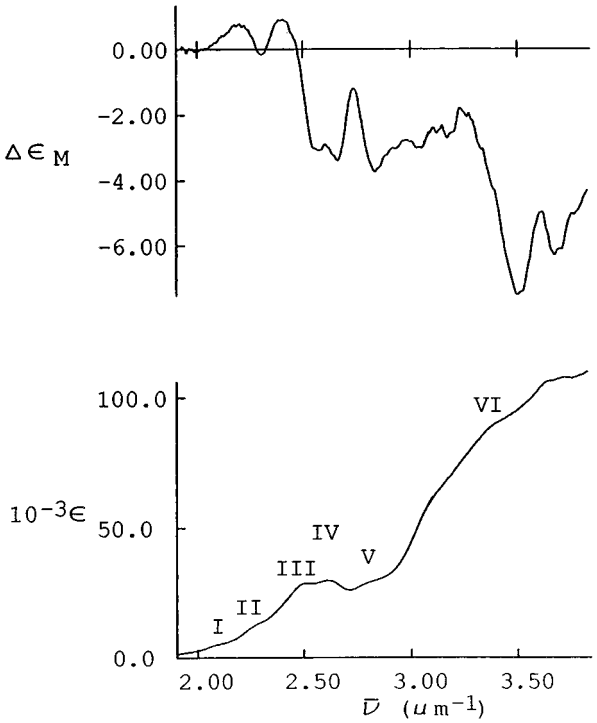

Figure 6. Magnetic circular dichroism (upper curve) and electronic absorption (lower curve) spectra for $[Pt(HgCl)_2(AuPPh_3)_8](BF_4)_2$ in acetonitrile at room temperature. The units are as in Figure 1.

Electronic Excited States and MCD Terms for MAu_8^{2+}. In order to develop an electronic structure model suitable for interpreting the absorption and MCD spectra for the Au cluster complexes, an MO energy level scheme was constructed for the MAu_8^{2+} ions. These ions were chosen partly because of their higher symmetry than some of the other Pt-centered Au complexes studied here and partly because the latter may be visualized as derivatives of $PtAu_8^{2+}$. The solution structures for the $PdAu_8^{2+}$ and $PtAu_8^{2+}$ ions are not known. Therefore in order to construct the MO scheme, a structural assumption must be made. The most reasonable assumption is that the solid-state D_{4d} skeletal structure **1** is retained when the solid compounds are dissolved in acetonitrile. In the discussion that follows the symmetry labels are those of D_{4d}. However, alternative structures were also considered and correlated with the D_{4d} structure. Two important symmetries that were considered were D_4 and D_{2h}. The latter corresponds to skeletal structure, **2**, observed for the Au_9^{3+}complex and is necessary for comparison purposes. A reduction of the D_{4d} symmetry to D_4 can be easily visualized by a small twist of one of the square faces of **1** relative to the other about the 4-fold axis; such a twist for small angles is expected to involve only a small change in the potential energy. Other more drastic distortions of the D_{4d} skeletal structure were considered less likely on energetic grounds.

The MO energy level scheme was developed by first forming Hückel MO's (HMO) for a hypothetical crown-shaped Au_8^{2+} cluster complex of D_{4d} symmetry. The MO's for the gold framework were formulated in terms of 6s valence orbitals by following the earlier study of Au_9^{3+} [12a] and by assuming bonding only between adjacent Au atoms. As in the case of Au_9^{3+}, the Au 5d orbitals are considered to be too stable to contribute appreciably to Au−Au bonding and the Au 6p orbitals are expected to be too high in energy. The Au_8^{2+} MO's were then extended to give the centered crown by the interaction of the central Pd(0) and Pt(0) atoms with the Au_8^{2+} skeleton. The Pd 5s and the Pt 6s orbitals were also assumed to have the greatest overlap with the Au 6s orbitals. The Pd 4d and Pt 5d orbitals, like the Au 5d orbitals, are visualized as essentially nonbonding with respect to the cluster framework. The HMO energy levels for the $PdAu_8^{2+}$ and $PtAu_8^{2+}$ complexes that result in D_{4d} are shown in Figure 7, while one-electron wavefunctions are given in Table 2. It should be emphasized that the MO enegy levels presented in Figure 7 are *schematic* and that no quantitative rigor is implied. Note the elaboration of the MO scheme for the central metal *n*d orbitals. Although not visualized as being strongly involved in bonding, these orbitals are believed to be important spectroscopically for Pt (see below). The framework e_1, e_2, e_3, b_2, and $2a_1$ MO's are assumed to be primarily Au centered. Even though the intermixing of the *n*d orbitals on the central atom with the framework MO's of the same symmetry type is permitted, this intermixing is taken to be small to a first approximation. The diamagnetic ground-state electron configuration is ... $(e_1)^4$ for both $PdAu_8^{2+}$ and $PtAu_8^{2+}$ and is designated $^1A_1$. Electric-dipole-allowed transitions are permitted to B_2 (*z*-polarized) and E_1 (*x*,*y*-polarized) excited states in D_{4d} (in D_4 they are A_2 and E, respectively). The lowest energy excited configurations which give allowed excited states are collected in Table 3. Transitions from the HOMO e_1 to the e_2, e_3, b_2, or $2a_1$ levels are appropriately designated *intraframework* (IF) Au_8^{2+} transitions in Table 3. Figure 8 shows an energy level correlation diagram between D_{4d}, D_4, and D_{2h}. If there is structural distortion from D_{4d} to D_4, transitions to formally D_{4d} symmetry-forbidden A_2 and E_3 excited states become symmetry-allowed A_2 and E excited states in D_4. Transitions to these states are expected to be weaker and may be partly obscured by the more intense allowed transitions to the B_2 and E_1 D_{4d} states (A_2 and E in D_4), which are allowed in both symmetries. Finally, transitions to formally spin-forbidden triplet states can give rise to intensity because of the intermixing of singlet and triplet excited states as a result of heavy atom Au or Pt spin−orbit coupling. The spin−orbit states for both D_{4d} and D_4 are listed in Table 3; spin−orbit states for D_{2h} were given earlier.[12a]

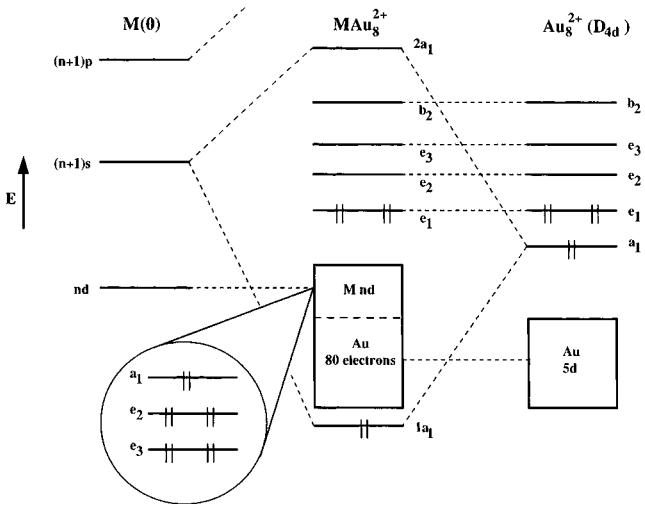

Figure 7. Schematic molecular orbital energy levels for $PdAu_8^{2+}$ and $PtAu_8^{2+}$, assuming D_{4d} symmetry and Pd 5s and Pt/Au 6s framework bonding.

The MCD spectra for $PdAu_8^{2+}$ and $PtAu_8^{2+}$ can exhibit both *A* terms (E_1 states), which result from Zeeman splitting of degenerate states, and *B* terms (B_2 and E_1 states), which result from mixing between states in the presence of the magnetic field.[19] The *A* and *B* terms for E_3 states may also be seen if the

(19) Piepho, S. B.; Schatz, P. N. *Group Theory in Spectroscopy with Applications to Magnetic Circular Dichroism;* Wiley-Interscience: New York, 1983. This reference describes the standard (Stephens) definitions and conventions that are used here.

Table 1. Spectral Data for Acetonitrile Solution

	absorption			MCD			absorption			MCD	
band no.	$\bar{\nu}$, μm^{-1}	λ, nm	ϵ, $(M\ cm)^{-1}$	ν, μm^{-1}	$\Delta\epsilon_M$, $(M\ cm\ T)^{-1}$	band no.	$\bar{\nu}$, μm^{-1}	λ, nm	ϵ, $(M\ cm)^{-1}$	ν, μm^{-1}	$\Delta\epsilon_M$, $(M\ cm\ T)^{-1}$
					$[Pd(AuPPh_3)_8](NO_3)_2$						
				1.69	−0.155					2.80	−2.03[a]
I	1.94	516	7 150[a]	1.99	+1.39	IV	2.88	347	61 800	2.91	−7.35
II	2.17	462	14 400	2.08	+1.19	V	3.24	309	65 100[a]	3.07	+2.54
				2.21	−2.77[a]					3.31	−10.3
III	2.42	414	22 000	2.31	−5.04	VI	3.36	290	67 800	3.38	−1.58
				2.50	+2.55						
					$[Pt(AuPPh_3)_8](NO_3)_2$						
				1.84	−1.21[a]	IV	2.82	354	47 500	2.84	−4.30
				1.95	−1.76	V	3.00	333	40 000[a]	3.04	+1.87
I	2.09	478	8 200[a]	2.11	+3.21					3.15	−1.71
				2.24	+1.71[a]	VI	3.27	306	72 300	3.21	+0.992
II	2.34	428	20 000	2.32	+2.93					3.32	−7.46
III	2.53	396	17 100[a]	2.50	−3.00	VII	3.50	286	75 100	3.51	−10.4
				2.71	−4.13						
					$[Pt(CO)(AuPPh_3)_8](NO_3)_2$						
				2.18	+0.430					2.94	−0.674
I	2.31	433	17 000	2.31	−0.328					3.23	−5.18
				2.43	+0.470	III	3.38	296	84 000[a]	3.40	+0.208
II	2.82	354	18 400[a]	2.70	−1.48	IV	3.52	284	91 600	3.60	−6.41
					$[Pt(AgNO_3)(AuPPh_3)_8](NO_3)_2$						
				1.82	−1.33[a]	IV	2.85	351	36 400[a]	2.82	−2.52
				1.90	−2.34	V	3.05	328	46 700	2.96	−0.830
I	2.08	480	6 590[a]	2.08	+3.00					3.12	−2.18
II	2.33	429	20 700	2.30	+2.71	VI	3.31	302	63 700[a]	3.32	−3.13
III	2.67	375	24 900[a]	2.67	−2.25	VII	3.51	285	74 400[a]	3.51	−9.49
					$[Pt(CuCl)(AuPPh_3)_8](NO_3)_2$						
				1.83	−1.48[a]	IV	2.82	354	47 900	2.83	−4.64
				1.95	−2.02	V	3.00	333	40 000[a]	3.05	+1.48
I	2.09	478	7 270[a]	2.11	+3.89	VI	3.27	306	73 000	3.23	+0.909
II	2.33	429	19 900	2.31	+3.30					3.33	−8.65
III	2.53	396	16 800[a]	2.51	−3.41	VII	3.50	286	75 500	3.52	−11.4
					$[Pt(AuP(p\text{-}tolyl)_3)_8](NO_3)_2$						
				1.81	−1.46[a]	IV	2.81	356	49 700	2.82	−3.80
				1.95	−2.35	V	3.06	327	42 400[a]	3.04	+2.90
I	2.09	479	7 560[a]	2.11	+4.42	VI	3.27	306	75 100	3.25	−0.940
II	2.33	430	20 000	2.30	+3.99					3.33	−8.89
III	2.52	397	17 000[a]	2.49	−4.26	VII	3.50	286	81 000[a]	3.51	−13.3
					$[Pt(Hg)_2(AuPPh_3)_8](NO_3)_2$						
I	2.27	441	18 100[a]	2.23	−1.73	IV	2.94	340	37 800[a]	2.92	−6.23
				2.30	−1.11					3.10	−6.05
II	2.36	424	23 300	2.36	−2.95	V	3.26	307	82 900[a]	3.30	+2.04
III	2.53	395	25 400	2.56	−3.36	VI	3.50	286	110 000	3.53	−16.1
				2.72	+2.17						
					$[Pt(HgCl)_2(AuPPh_3)_8](BF_4)_2$						
I	2.11	475	5 320[a]	2.20	+0.783	V	2.84	352	30 100[a]	2.83	−3.73
II	2.31	433	14 100[a]	2.30	−0.153					3.04	−2.97
III	2.51	399	28 600	2.40	+0.880					3.17	−2.73
				2.57	−3.06	VI	3.41	293	87 100[a]	3.24	−1.79
IV	2.61	383	29 900	2.66	−3.42					3.50	−7.51
					$[Pt(HgNO_3)_2(AuPPh_3)_8](BF_4)_2$						
I	2.09	479	4 900[a]	2.08	+0.089	V				2.83	−3.06
II	2.32	430	13 000[a]	2.31	−0.751					3.03	−3.48
III	2.53	395	24 000[a]	2.43	+0.30	VI	3.41	293	91 000[a]	3.23	−0.98
				2.58	−2.28[a]					3.49	−6.96
IV	2.65	378	25 000[a]	2.66	−2.72						

[a] Shoulder.

symmetry is reduced to D_4. The diamagnetic ground state requires *C* terms to be absent. For space-averaged anisotropic molecules in solution, MCD *A* terms for the degenerate $E_1(i)$ excited states can be described[19] by the $\bar{A}_1/\bar{D}_0$ parameter ratio in eq 1, where D_0, the electric-dipole strength of the transition

$$\bar{A}_1/\bar{D}_0 = \left(\frac{-1}{\sqrt{2}\mu_B}\right)\langle E_1(i)||\mu^{A_2}||E_1(i)\rangle \qquad (1)$$

to the $E_1(i)$ states, is given by $D_0 = (^1/_3)\ |\langle {}^1A_1||\mathbf{m}^{E_1}||E_1(i)\rangle|^2$ and μ_B = Bohr magneton; $\mathbf{m} = e\mathbf{r}$ and $\mu = -\mu_B(\mathbf{L} + 2\mathbf{S})$ are the electric and magnetic moment operators in the respective reduced matrix elements (RME). Defined in terms of antisymmetrized one-electron MO's, the $E_1(i)$ states (Table 3) can be approximated by Pd or Pt and Au atomic orbitals. In order to estimate the sign of $\bar{A}_1/\bar{D}_0$ for Au-localized orbitals to a first approximation using eq 1, two-centered integrals are required

Table 2. One-Electron Molecular Orbitals for MAu_8^{2+}

sym	energy[a]	MO wavefunction[b]
$1a_1$[c]	$2\sqrt{2}\beta_1 + \beta_2$	$^1/_4(2\sqrt{2}\phi_1 + \phi_2 + \phi_3 + \phi_4 + \phi_5 + \phi_6 + \phi_7 + \phi_8 + \phi_9)$
e_1	$\sqrt{2}\beta_2$	$\frac{1}{2\sqrt{2}}(\sqrt{2}\phi_2 - \sqrt{2}\phi_4 + \phi_6 - \phi_7 - \phi_8 + \phi_9)$
		$\frac{1}{2\sqrt{2}}(-\sqrt{2}\phi_3 + \sqrt{2}\phi_5 - \phi_6 - \phi_7 + \phi_8 + \phi_9)$
e_2	0	$^1/_2(\phi_2 - \phi_3 + \phi_4 - \phi_5)$
		$^1/_2(\phi_6 - \phi_7 + \phi_8 - \phi_9)$
e_3	$-\sqrt{2}\beta_2$	$\frac{1}{2\sqrt{2}}(\sqrt{2}\phi_2 - \sqrt{2}\phi_4 - \phi_6 + \phi_7 + \phi_8 - \phi_9)$
		$\frac{1}{2\sqrt{2}}(-\sqrt{2}\phi_3 + \sqrt{2}\phi_5 + \phi_6 + \phi_7 - \phi_8 - \phi_9)$
b_2	$-2\beta_2$	$\frac{1}{2\sqrt{2}}(\phi_2 + \phi_3 + \phi_4 + \phi_5 - \phi_6 - \phi_7 - \phi_8 - \phi_9)$
$2a_1$[c]	$-2\sqrt{2}\beta_1 + \beta_2$	$^1/_4(2\sqrt{2}\phi_1 - \phi_2 - \phi_3 - \phi_4 - \phi_5 - \phi_6 - \phi_7 - \phi_8 - \phi_9)$

[a] Hückel MO exchange integrals: β_1 from radial overlap of ϕ_1 with ϕ_2, ϕ_3, ... ϕ_9; β_2 from adjacent tangential overlap ϕ_2, ϕ_9; ϕ_9, ϕ_5; etc. [b] ϕ_1 = Pt 6s or Pd 5s orbital; ϕ_i = Au 6s orbital on atom i ($i > 1$). [c] For the hypothetical Au_8^{2+} (D_{4d}) cluster, this energy level is omitted while the energy of $1a_1$ becomes $+2\beta_2$ with the omission of ϕ_1 from the $1a_1$ wavefunction.

Table 3. Excited Configurations and States

excited confgn.[a]	zero-order states	spin−orbit states in D_{4d}[b]	spin−orbit states in D_4[b]	*A* term sign[c]	excited confgn.[a]	zero-order states	spin−orbit states in D_{4d}[b]	spin−orbit states in D_4[b]	*A* term sign[c]
				Intraframework (IF) Au_8^{2+}					
$e_1^3e_2$	$^1E_1$	$1E_1$	1E	positive	$2a_1e_2$[f]	$^1E_2$	($12E_2$)	($12B_1$), ($12B_2$)	
	$^3E_1$	$2E_1$	2E	positive		$^3E_2$	$15E_1$	25E	negative
		$1B_2$	$1A_2$				($11E_3$), ($13E_2$)	26E, ($13B_1$), ($13B_2$)	negative
		($1B_1$), ($1E_2$)	($1A_1$), ($1B_1$), ($1B_2$)		$2a_1e_3$[f]	$^1E_3$	($12E_3$)	27E	positive
	$^1E_3$	($1E_3$)	3E	positive		$^3E_3$	($13E_3$)	28E	positive
	$^3E_3$	($2E_3$)	4E	positive			($6A_2$)	$14A_2$	
		($1A_2$)	$2A_2$				($6A_1$), ($14E_2$)	($14A_1$), ($14B_1$), ($14B_2$)	
		($1A_1$), ($2E_2$)	($2A_1$), ($2B_1$), ($2B_2$)		$2a_1b_2$[f]	$^1B_2$	$9B_2$	$15A_2$	
$e_1^3e_3$	$^1B_1$	($2B_1$)	($3A_1$)			$^3B_2$	$16E_1$	29E	negative
	$^3B_1$	$3E_1$	5E	positive			($9B_1$)	($15A_1$)	
		$2B_2$	$3A_2$		$2a_1a_1$[f]	$^1A_1$	($7A_1$)	$16A_1$	
	$^1B_2$	$3B_2$	$4A_2$			$^3A_1$	($14E_3$)	30E	positive
	$^3B_2$	$4E_1$	6E	positive			($7A_2$)	$16A_2$	
		($3B_1$)	($4A_1$)		$1b_2a_1$[e]	$^1B_2$	$10B_2$	$17A_2$	
	$^1E_2$	($3E_2$)	($3B_1$), ($3B_2$)			$^3B_2$	$17E_1$	31E	negative
	$^3E_2$	$5E_1$	7E	~0			($10B_1$)	($17A_1$)	
		($3E_3$), ($4E_2$)	8E, ($4B_1$), ($4B_2$)		$1b_2e_2$[f]	$^1E_2$	($15E_2$)	($15B_1$), ($15B_2$)	
$e_1^3b_2$	$^1E_3$	($4E_3$)	9E	negative		$^3E_2$	$18E_1$	32E	negative
	$^3E_3$	($5E_3$)	10E	negative			($15E_3$), ($16E_2$)	33E,($16B_1$), ($16B_2$)	negative
		($2A_2$)	$5A_2$		$1b_2e_3$[f]	$^1E_1$	$19E_1$	34E	negative
		($2A_1$), ($5E_2$)	($5A_1$), ($5B_1$), ($5B_2$)			$^3E_1$	$20E_1$	35E	negative
$e_1^3 2a_1$	$^1E_1$	$6E_1$	11E	negative			$11B_2$	$18A_2$	
	$^3E_1$	$7E_1$	12E	negative			($11B_1$), ($17E_2$)	($18A_1$), ($17B_1$), ($17B_2$)	
		$4B_2$	$6A_2$		$1b_2b_2$[f]	$^1A_1$	($8A_1$)	($19A_1$)	
		($4B_1$), ($6E_2$)	($6A_1$), ($6B_1$), ($6B_2$)			$^3A_1$	($16E_3$)	36E	positive
$e_1^3 2a_1$[e]	$^1E_1$	$13E_1$	23E	negative			($8A_2$)	$19A_2$	
	$^3E_1$	$14E_1$	24E	negative	$1b_23a_1$[f]	$^1B_2$	$12B_2$	$20A_2$	
		$8B_2$	$13A_2$			$^3B_2$	$21E_1$	37E	negative
		($8B_1$), ($11E_2$)	($13A_1$), ($11B_1$), ($11B_2$)				($12B_1$)	($20A_1$)	
				Pt 5d → Au 6s[d]					
a_1(Pt)e_2	$^1E_2$	($7E_2$)	($7B_1$), ($7B_2$)				$5B_2$	$9A_2$	
	$^3E_2$	$8E_1$	13E	negative		$^1B_2$	$6B_2$	$10A_2$	
		($6E_3$)	14E	negative		$^3B_2$	$10E_1$	18E	positive
		($8E_2$)	($8B_1$), ($8B_2$)				($6B_1$)	($10A_1$)	
e_2(Pt)$^3e_2$	$^1A_1$	($3A_1$)	($7A_1$)		e_2(Pt)$^3e_3$	$^1E_1$	$11E_1$	19E	negative
	$^3A_1$	($7E_3$)	15E	positive		$^3E_1$	$12E_1$	20E	negative
		($3A_2$)	$7A_2$				$7B_2$	$11A_2$	
	$^1A_2$	($4A_2$)	$8A_2$				($7B_1$), ($9E_2$)	($11A_1$), ($9B_1$), ($9B_2$)	
	$^3A_2$	($8E_3$)	16E	positive		$^1E_3$	($9E_3$)	21E	negative
		($4A_1$)	($8A_1$)			$^3E_3$	($10E_3$)	22E	negative
	$^1B_1$	($5B_1$)	($9A_1$)				($5A_2$)	$12A_2$	
	$^3B_1$	$9E_1$	17E	positive			($5A_1$), ($10E_2$)	($12A_1$), ($10B_1$), ($10B_2$)	

[a] Filled orbitals omitted, notation as in Figure 5. Ground state confign: ... e_1^4, $^1A_1$. [b] Electric-dipole-forbidden states in parentheses. [c] Estimated from eq 1 for E_1 states (or E states in D_4). [d] a_1(Pt) = Pt $5d_{z^2}$, e_3(Pt) = Pt $5d_{xz}$, $5d_{yz}$, e_2(Pt) = Pt $5d_{xy}$, $5d_{x^2-y^2}$. [e] For the $Pt(HgCl)_2Au_8^{2+}$ complex only, notation as in Figure 9. Ground-state configuration: ... e_1^4, $^1A_1$. [f] For the $Pt(Hg)_2Au_8^{2+}$ complex, notation as in Figure 9. Ground-state configuration: ... $e_1^4 2a_1^2$, $^1A_1$.

for the orbital (**L**) part of the magnetic moment RME because the one-center terms are zero due to the lack of angular momentum for the Au 6s orbitals. For the approximate evaluation of the RME of the spin−orbit states of $1E_1$ through

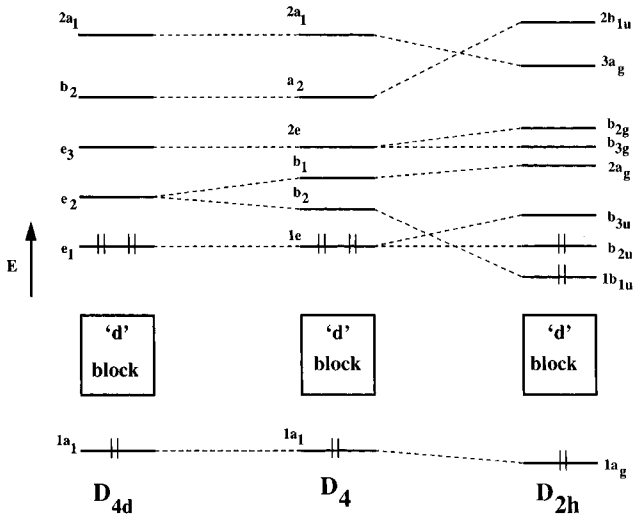

Figure 8. Molecular orbital energy correlation diagram among the symmetries of D_{4d}, D_4, and D_{2h}.

$7E_1$ (1E through 12E for D_4), the two-centered terms were evaluated using eq 2, where ϕ_i represents the 6s orbital on the appropriately numbered atom (see footnote b in Table 2), and R_{x_j} is the *x* coordinate of the vector from the origin to atom *j*.

$$\langle \phi_i | l_{z_j} | \phi_j \rangle = -i\hbar R_{x_j} \left\langle \phi_i \left| \frac{\partial}{\partial_{y_j}} \right| \partial_j \right\rangle \qquad (2)$$

The *sign* of the MCD *A* term for the $E_1(i)$ excited states, found by using eq 1, is included in Table 3. Because of the several approximations involved, the quantitative magnitude of the $\bar{A}_1/\bar{D}_0$ ratios determined from eq 1 is not deemed very reliable.

The MCD *B* terms expected for the transitions $^1A_1 \rightarrow J$, where J is either a $B_2(i)$ or an $E_1(i)$ state, arise from the summation of the magnetic field induced mixing with all other K excited states, where $K = E_1(j)$ for $J = B_2(i)$ and $K = B_2(j)$ or $E_1(j)$ for $J = E_1(i)$. The *B* term for $^1A_1 \rightarrow J$ is given by eq 3,[19] where ΔW_{KJ}

$$\bar{B}_0(J,K) = \mathrm{Re}\left\{ \frac{2a}{3\mu_B} \left[\sum_{K \neq J} \frac{\langle J||\mu||K\rangle}{\Delta W_{KJ}} \langle A_1||\mathbf{m}||J\rangle\langle K||\mathbf{m}||A_1\rangle \right] \right\} \qquad (3)$$

$= W_K - W_J$ is the energy difference between states K and J, and $a = -1/\sqrt{2}$ for J, $K = E_1$ and $a = +1$ for $J = E_1$ and $K = B_2$. Because the summation is over all states K, the determination of *B* term signs and magnitudes requires a detailed knowledge of the relative energies of the J and K states and, thus, is very difficult. However the inverse energy dependence in the summation over K states in eq 3 dictates that the largest contributions to the *B* term for the transition to the state J will be from states K closest in energy to J. Therefore if the summation can be reduced to one or only a few terms from states very close in energy, then an estimate of the *B* term sign can sometimes be made. In the present case, for example, a *B* term sign estimate was carried out for $J = 1E_3(^1E_3)$ and $K = 1E_1(^1E_1)$ excited states (see Table 3 for electronic state notation) and was found to be *positive*. Similarly, the *B* term contribution for $J = 1E_1(^1E_1)$ and $K = 3B_2(^1B_2)$ (K state) was found to be *positive*, also. However, due to the complexity of the present case which results from many possible close-lying states in the summation, it was concluded that a reliable prediction of *B* term signs was, *in general*, not feasible, especially for states of intermediate energy with contributions from both lower and higher energy states.

Spectral Interpretation for the MAu_8^{2+} Ions. The electronic absorption and MCD spectra below $\sim 3.5\ \mu m^{-1}$ are assigned to intramolecular transitions within the cluster complex. Most assignments have been chosen on the basis of band energy and intensity, within the context of the lowest energy excited configurations and states (Table 3), together with the predicted MCD term signs. The following discussion offers a rationale for specific spectral assignments.

$PdAu_8^{2+}$ Spectra. Bands I−III are assigned as IF transitions to states of the lowest energy $e_1^3e_2$ configuration. Bands II and III are assigned as transitions to the $1E_3(^1E_3)$ and $1E_1(^1E_1)$ states, respectively, which are the lowest energy excited states of singlet origin, while the weaker band I is assigned as transitions to the states of triplet origin, $2E_3(^3E_3)$ and $1A_2(^3E_3)$. The transition to the $1E_1(^1E_1)$ state, allowed in both D_{4d} and D_4 symmetries, is expected to have a greater absorption intensity than the transition to the $1E_3(^1E_3)$ state, allowed in only D_4 symmetry. Consistent with the assignment for band III, the MCD spectrum for $PdAu_8^{2+}$ shows a positive *A* term, although it is unsymmetrical and broadened on the low-energy side. The transition to the $1E_1(^1E_1)$ state is also predicted to have a negative *B* term contribution from the magnetically coupled lower energy $1E_3(^1E_3)$ state (band II). The unsymmetrical appearance of the *A* term for band III is believed to be partly due to this negative *B* term. The broadness may be due to overlap with the MCD features in the region of band II. The MCD spectrum for band II is interpreted as presenting a dominant contribution from the positive *B* term from the $1E_3(^1E_3)$ state (see above) which must obscure the positive *A* term expected for the transition to this state. Transitions to the $1B_2(^3E_1)$ and $2E_1(^3E_1)$ states are also expected lower in energy than band III, near the energy of band II, and thus may contribute to the modest absorption intensity seen for this band. These transitions are predicted to have negative *B* term contributions from the magnetically coupled lower energy $2E_3(^3E_3)$ state (band I; see below), which together with the positive *B* term for the $1E_3(^1E_3)$ state could give the MCD spectrum for $PdAu_8^{2+}$ the appearance of a negative pseudo-*A* term (*B* terms of opposite signs close together)[19] in the region of band II. At low energy, the broad shoulder band I is assigned to unresolved transitions to the predominantly triplet states $2E_3(^3E_3)$ and $1A_2(^3E_3)$ on the basis of their lower energy position compared to the singlet $1E_3(^1E_3)$ state, band II. The MCD spectrum in the region of band I appears to be dominated by a positive *B* term with a minor contribution from a small positive *A* term responsible for the weak negative MCD minimum at $1.69\ \mu m^{-1}$, which is lower in energy than the absorption shoulder at $1.94\ \mu m^{-1}$. The positive *A* term is consistent with the $2E_3(^3E_3)$ assignment for band I, and a positive *B* term is expected for the magnetic interaction of $2E_3(^3E_3)$ with $1B_2(^3E_1)$ and $2E_1(^3E_1)$, which, as noted above, are likely to be near the energy of band II. The *B* term for the transition to the $1A_2(^3E_3)$ state, however, is of undetermined sign.

The MCD spectrum in the region of band IV shows a single minimum at nearly the same energy ($2.91\ \mu m^{-1}$) as the intense absorption maximum ($2.88\ \mu m^{-1}$) and therefore is interpreted as a negative *B* term. Band IV is therefore reasonably assigned to the transition to $3B_2(^1B_2)$, the only fully allowed, singlet, and nondegenerate state of the next lowest energy configuration, $e_1^3e_3$. The large negative MCD intensity for band IV is assumed to be due to magnetic coupling to higher energy states beyond the range of measurement. At slightly lower energy a negative MCD shoulder at $2.80\ \mu m^{-1}$, which has no resolved absorption, may signal the presence of a transition to the $4E_1(^3B_2)$ state which is expected to be lower in energy compared to its singlet counterpart $3B_2(^1B_2)$.

Band V is assigned to the transition to the higher energy $6E_1(^1E_1)$ state, of the $e_1^3 2a_1$ energy configuration. The MCD spectrum is interpreted as showing a negative *A* term in accord with expectation. However the *A* term is unsymmetrical due to overlap with adjacent transitions. Figure 1 shows that there is a broad shoulder on the low-energy side of band V which indicates the presence of several unresolved transitions. For example, the transitions to the $4E_3(^1E_3)$, $5E_3(^3E_3)$, and $2A_2(^3E_3)$ states from the lower energy $e_1^3 b_2$ configuration are expected to not only give negative *A* terms (E_3 states) and *B* terms of undetermined sign but to be weak since they are only allowed in D_4 symmetry. The transition to the $7E_1(^3E_1)$ and $4B_2(^3E_1)$ states of triplet parentage are also expected to be weaker and lower in energy than band V and predicted to have a negative *A* term and a *B* term of undetermined sign, respectively. The combination of all of these unresolved weak *A* and *B* terms may explain why the *A* term for band V is unsymmetrical. Finally, the assignment of band VI is not easily made. One possibility is to an IF Au_8^{2+} transition from a higher energy configuration such as from a Au 5d orbital to the Au 6s orbitals. Unfortunately the MCD results offer little help, since a term assignment is not clear from the observed spectrum.

The assignments of the absorption and MCD spectra for Au_9^{3+} complex were based on IF Au_8^{2+}transitions even though the skeletal structure was assumed to be different (i.e., **2**, D_{2h}).[12a] The low-energy region of the MCD spectrum for $PdAu_8^{2+}$, in fact, looks similar in pattern to that reported for Au_9^{3+} (Figure 1, ref 12a), with the bands of $PdAu_8^{2+}$ shifted $\sim$0.4 μm^{-1} to lower energy. The assignments for bands I−IV for both $PdAu_8^{2+}$ and Au_9^{3+} may be correlated by using Figure 8, and the excited configurations for each band for both complexes are found to be essentially the same. Minor changes between the spectra for $PdAu_8^{2+}$ and that of Au_9^{3+} certainly would be expected upon replacing the center Pd(0) with Au(I) and altering the skeletal structure. Thus it appears that a satisfactory interpretation of the lower energy absorption and MCD spectra for $PdAu_8^{2+}$, like that of Au_9^{3+}, can be made primarily on the basis of the IF Au_8^{2+}type transitions.

$PtAu_8^{2+}$ Spectra. When a comparison is made between the absorption and MCD spectra for $PtAu_8^{2+}$ with that of $PdAu_8^{2+}$ or Au_9^{3+} at energies greater than 2.6 μm^{-1}, especially for band IV (in all three), and between band VI ($PtAu_8^{2+}$) and band V ($PdAu_8^{2+}$), similarities are seen which suggest common assignments, namely, that these $PtAu_8^{2+}$ transitions are also primarily due to IF Au_8^{2+} transitions. Thus, band IV at 2.82 μm^{-1} is assigned to the transition to $3B_2(^1B_2)$, with the MCD minimum at 2.84 μm^{-1} interpreted as a negative *B* term. Band VI is assigned to the transition to the higher energy $6E_1(^1E_1)$ state. Weaker band III is reasonably assigned to the transition to the predominantly triplet state $4E_1(^3B_2)$, on the basis of its energy and intensity, which is lower than the singlet state $3B_2(^1B_2)$ from the same configuration. The negative MCD feature at 2.71 μm^{-1} can be assigned to the transition to the $5E_1(^3E_2)$ state, on the basis of its energy; the absorption is unresolved. Band V, also of low intensity, is assigned similarly to a state of triplet parentage, $4B_2(^3E_1)$, with the MCD interpreted as a *B* term. The negative MCD feature at 3.15 μm^{-1} can be assigned to the transition to $7E_1(^3E_1)$ state on the basis of its proximity to $4B_2(^3E_1)$ and its lower energy compared to $6E_1(^1E_1)$ (band VI); the absorption is also unresolved. Band VII may signal a higher energy 5d IF Au_8^{2+} transition, but the proximity to phenyl absorptions makes assignments in this region difficult. For example, the large negative MCD feature at 3.51 μm^{-1} probably results from the onset of strong negative MCD signals from the triphenylphosphine ligands.[20]

If assignments of IF transitions for $PtAu_8^{2+}$ are made at energies > 2.6 μm^{-1}, it follows that the lower energy IF transitions assigned in the spectra for $PdAu_8^{2+}$ or Au_9^{3+} *must also be present* in the regions of bands I and II for $PtAu_8^{2+}$. However, the $PtAu_8^{2+}$ MCD spectrum in this region is quite different compared to the MCD spectra for $PdAu_8^{2+}$ and Au_9^{3+}, even though the absorption spectra for all three are similar. Therefore, other transitions must be present *in addition* to the IF transitions for $PtAu_8^{2+}$ to account for the differences observed in the MCD. One reasonable possibility is the presence of Pt 5d → framework Au 6s charge-transfer-like transitions in the low-energy region. Consideration of atomic orbital energies place the Pt(0) 5d orbitals higher in energy than the 5d orbitals for Au(+0.25).[21] The transitions from the Pt 5d orbitals to Au 6s orbitals are expected to be less intense than the IF Au_8^{2+} transitions due to the ratio of Pt to Au and are thus likely to be obscured by the latter in the absorption spectrum. Yet the greater relative intensities of the MCD features in the experimental spectrum are consistent with the angular momentum of the Pt 5d orbitals which lead to higher excited state magnetic moments (single-center terms in eq 1). Thus, the Pt → Au transition to the $9E_1(^3B_1)$ state and/or $10E_1(^3B_2)$ state, both of triplet origin, can be envisioned in the region of band I. The positive *A* term for both of these states would complement the small positive *A* term for the $1E_3(^1E_3)$ IF state assumed to be in the same region. Also, the negative MCD shoulder at 1.84 μm^{-1} may signal the beginning of another positive *A* term expected for the Pt → Au transition to $7E_3(^3A_1)$ and/or $8E_3(^3A_2)$. The absorption for both of these transitions is expected to be very weak, and the MCD *A* terms are predicted to be positive, which would add to the positive *A* term for the $2E_3(^3E_3)$ IF state assumed to be present also in the region of the broad unresolved absorption on the low-energy side of band I. Furthermore, the Pt → Au transition to the $11E_1(^1E_1)$ state can be envisioned in the region of band II. The negative *A* term predicted for $11E_1(^1E_1)$ is then interpreted as dominating the MCD spectrum and obscuring the weaker positive *A* term expected for the IF transition to the $1E_1(^1E_1)$ state which is believed to be present at similar energy. Thus the presence of Pt → Au transitions in the region of bands I and II for $PtAu_8^{2+}$ provides an explanation for the observed differences in the MCD spectrum compared to $PdAu_8^{2+}$ and Au_9^{3+}. Finally, band III has a lower relative intensity in the absorption spectrum for $PtAu_8^{2+}$ and increased complexity in the MCD spectrum which may also signal the presence of one or more additional Pt → Au transitions, perhaps to the $9E_3(^1E_3)$ and $10E_3(^3E_3)$ states, together with the IF transition to $4E_1(^3B_2)$ believed to be present.

$Pt(CO)Au_8^{2+}$ Structure and Spectra. This strongly colored complex has a skeletal structure,[9] **3** in the solid state, with

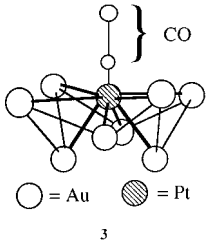

3

approximately C_{2v} symmetry. Compared to **1**, the Pt atom is drawn up out of the center of the Au_8^{2+} ring, distorting the ring

(20) Adrowski, M. J.; Mason, W. R. Unpublished results, 1994. The absorption for free PPh_3 in acetonitrile begins around 3.50 μm^{-1} and shows a prominent negative MCD feature at $\sim$3.8 μm^{-1}.

(21) Moore, C. E. *Natl. Bur. Stand. Circ. (U.S.)* **1958**, *No. 467*, Vol. III.

slightly. The Pt−C distance of 1.896 Å is not unusual for a Pt−CO bond, while the Au−C distances are approximately 3.0 Å, which are considered to be too long for bonding. The Pt−Au distances are increased slightly compared to $PtAu_8^{2+}$. The solution structure of the $Pt(CO)Au_8^{2+}$ complex is not known, and the solid state C_{2v} skeletal symmetry (*z* axis along the Pt−C bond) is assumed to be retained in solution. A simple HMO treatment of **3** was developed by adding the σ(filled) and π*-(empty) energy levels of the CO ligand to the scheme for $PtAu_8^{2+}$, with due allowance for the reduction in symmetry.[22] The Pt d π orbitals for the $Pt(CO)Au_8^{2+}$ complex in C_{2v} are expected to be stabilized due to a back-bonding interaction with the π* orbitals of the CO, while the Au-based orbitals are expected to be only slightly affected. Thus, the lowest energy excited states are expected to be IF Au_8^{2+}. In contrast, the Pt → Au transitions for the $PtAu_8^{2+}$ complex should be shifted to higher energy in the spectra for the $Pt(CO)Au_8^{2+}$ complex where they will likely be obscured by more intense IF Au_8^{2+} transitions. The MCD spectra for the C_{2v} $Pt(CO)Au_8^{2+}$ complex can exhibit only *B* terms, resulting from magnetic coupling of nondegenerate excited states.[19] Even though the reliable *a priori* prediction of *B* term signs is in general very difficult, the pattern of features in the MCD can be used to assist in making assignments. For example, correlations and comparisons of the spectra for the $Pt(CO)Au_8^{2+}$ complex with the spectra for the $PdAu_8^{2+}$ complex shows that certain features ascribed to the IF Au_8^{2+} transitions are only affected slightly between the two complexes. In view of the many allowed possible excited states and the few visible bands in the absorption spectrum, the interpretation of the $Pt(CO)Au_8^{2+}$ spectra must be qualitative.

Due to the broad nature of band I, Figure 3, and the positive and negative features of the MCD spectrum, several excited states must be present in this region. Band I is logically assigned to the unresolved transitions that correlate with the IF Au_8^{2+} transitions to the singlet degenerate excited states $1E_3(^1E_3)$, and $1E_1(^1E_1)$, assigned for bands II and III for the $PdAu_8^{2+}$ complex. Other IF transitions, allowed due to the lower symmetry for the $Pt(CO)Au_8^{2+}$ complex, may also be present in the region of band I, adding to its broadness. The corresponding triplet states will be lower in energy and account for the tail on the lower energy side of the absorption band. The MCD spectrum for the $Pt(CO)Au_8^{2+}$ complex at energies > ~3.0 μm^{-1} is remarkably similar to that of the $PdAu_8^{2+}$ complex and, to a lesser degree, to that of the $PtAu_8^{2+}$ complex for energies > ~2.8 μm^{-1}. The similarities argue for the same type of transitions in the spectra for the $Pt(CO)Au_8^{2+}$ complex. Therefore, band III is assigned to the IF transition to $3B_2(^1B_2)$ correlating with band IV in both the $PdAu_8^{2+}$ and $PtAu_8^{2+}$ complexes. The appearance of one broad band in the absorption spectrum for the $Pt(CO)Au_8^{2+}$ complex is consistent with increased congestion and compression of states compared to the absorption spectrum for the $PdAu_8^{2+}$ complex. Band IV is assigned by analogy to the assignment made for band VI for the $PtAu_8^{2+}$ complex. Higher energy IF Au_8^{2+} transitions and PPh_3 ligand transitions are probably responsible for the intensity in the absorption spectrum at energies > ~3.5 μm^{-1}. The unresolved absorption region to lower energy than band III for the $Pt(CO)Au_8^{2+}$ complex is likely due to a number of triplet states that are allowed in C_{2v}, but not in D_{4d}. For example, the triplet states originating from the excited configurations of $e_1^3b_2$ in D_{4d} would become allowed in C_{2v}. Also transitions to the excited states (in D_{4d}) $4E_1(^3B_2)$ and $5E_1(^3E_2)$, which were assigned for $PdAu_8^{2+}$ and $PtAu_8^{2+}$ complexes in the region between ~2.5 and 3.0 μm^{-1}, are logically expected in this same region because the singlets of the same configuration are assigned to band III for $Pt(CO)Au_8^{2+}$ to higher energy.

The MCD spectrum for the $Pt(CO)Au_8^{2+}$ complex, Figure 3, compared to that for $PtAu_8^{2+}$, Figure 2, clearly shows considerable differences. The dramatic change in the lower energy region in the MCD spectrum for $Pt(CO)Au_8^{2+}$ is consistent with the CO ligand primarily affecting the Pt → Au transitions. The IF Au_8^{2+} transitions, which should be relatively unaffected between $Pt(CO)Au_8^{2+}$ and $PtAu_8^{2+}$, remain mostly unchanged. The differences that do occur are likely due to differences in structure (C_{2v} vs. D_{4d}) and therefore small shifts in energy levels.

$Pt(AgNO_3)Au_8^{2+}$ and $Pt(CuCl)Au_8^{2+}$ Structures and Spectra. These Lewis acid adducts of $PtAu_8^{2+}$ have structures, **4**,

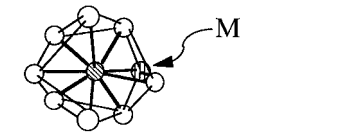

4

resembling the $PtAu_8^{2+}$ crown skeleton, with Ag or Cu atoms bonded to the side[14,15] among the crown Au atoms to give approximately C_s symmetry. The Pt−Ag bond distance is slightly longer than the Pt−Au distances, while the 3 Ag−Au distances are almost the same as the Au−Au distances. The Pt−Cu distance is roughly the same as the Pt−Au distances though the 3 Cu−Au distances are slightly shorter than the Au−Au distances found in the complex. The acetonitrile solution skeletal structures are presumed to be **4**, but the NO_3^- ligand on the Ag(I) may be partly dissociated. The presence or absence of coordinated NO_3^- will not likely affect the intramolecular electronic transitions attributed to the cluster complex (the NO_3^- ligand is included in the $Pt(AgNO_3)Au_8^{2+}$ formula in the following discussion).

Even though the Ag and Cu atoms are partly bound to the platinum atom in both the $Pt(AgNO_3)Au_8^{2+}$ and $Pt(CuCl)Au_8^{2+}$ complexes, the pattern in the lower energy region of the MCD spectra ascribed to the Pt → Au transitions in the $PtAu_8^{2+}$ complex seems to be very similar (see Figure 4 and Table 1, compared to Figure 2). This is reasonable because the locations of both the $AgNO_3$ and CuCl ligands primarily among the Au atoms are not expected to greatly affect the platinum 5d orbitals and, in turn, the Pt → Au transitions. Thus assignments made for bands I and II for the $PtAu_8^{2+}$ complex would apply in an analogous manner for both the $Pt(AgNO_3)Au_8^{2+}$ and $Pt(CuCl)Au_8^{2+}$ complexes. At higher energies, the absorption and MCD spectra for the $Pt(CuCl)Au_8^{2+}$ complex appear to be unaffected by the addition of the CuCl ligand into the ring of gold atoms. The IF Au_8^{2+} transitions that have been assigned to bands III through VII for the $PtAu_8^{2+}$ complex can be reasonably applied to those same bands for the $Pt(CuCl)Au_8^{2+}$ complex. For the $Pt(AgNO_3)Au_8^{2+}$ complex, the absorption and MCD spectra at higher energies (~2.5−3.5 μm^{-1}) are affected slightly by the addition of the $AgNO_3$ ligand. The IF transitions appear to be shifted closer together, which results in generally poorer resolution in the absorption and MCD spectrum in this region.

$Pt(AuP(p\text{-tolyl})_3)_8^{2+}$ Spectra. The structure of $Pt(AuP(p\text{-tolyl})_3)_8^{2+}$ is presumed to be **1**, the same as for $PtAu_8^{2+}$. The absorption and MCD spectra for $Pt(AuP(p\text{-tolyl})_3)_8^{2+}$ and $PtAu_8^{2+}$ are remarkably similar (see Table 1), which result argues for an analogous spectral interpretation. The additional electron density from the phosphine due to the *p*-tolyl groups apparently does not affect the relative orbital energies of the cluster complex.

(22) Adrowski, M. J. Dissertation, Northern Illinois University, 1996.

$Pt(Hg)_2Au_8^{2+}$ and $Pt(HgX)_2Au_8^{2+}$ ($X = Cl^-, NO_3^-$) Structures and States. The $Pt(Hg)_2Au_8^{2+}$ complex[1,16] and the $Pt(HgNO_3)_2Au_8^{2+}$ complex[1,17] (and presumably also the $Pt(HgCl)_2Au_8^{2+}$ complex[1,2,17]) have a molecular structure, **5**, which maintains the D_{4d} $PtAu_8^{2+}$crown skeletal configuration with Hg, $(NO_3)Hg-$, or ClHg− ligands residing above and below the Pt atom in the cluster. The average Hg−Au bond distance in $Pt(Hg)_2Au_8^{2+}$ and $Pt(HgNO_3)_2Au_8^{2+}$ is 3.00 Å, and the Hg−Pt bond distances are 2.98 Å. The average Pt−Au bond distances in the $PtAu_8^{2+}$ and $Pt(Hg)_2Au_8^{2+}$ complexes are all within the range 2.629−2.635 Å. In acetonitrile solution, the skeletal structures are assumed to be **5**, but for $Pt(HgNO_3)_2Au_8^{2+}$ the NO_3^- ligands, as in the case of $Pt(AgNO_3)Au_8^{2+}$ above, may be partly dissociated.[16,17] The electronic spectra are not expected to be affected by partial dissociation, and the NO_3^- ligands are retained in the formula to emphasize Hg(I) in the cluster complex.

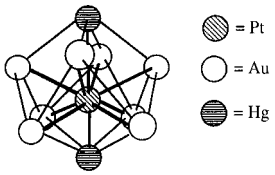

5

The absorption spectra for the $Pt(Hg)_2Au_8^{2+}$ and $Pt(HgX)_2Au_8^{2+}$ ($X = Cl^-, NO_3^-$) complexes are similar to each other (see Figures 5 and 6 and Table 1). However, the MCD spectra for the $Pt(Hg)_2Au_8^{2+}$ and the $Pt(HgX)_2Au_8^{2+}$ complexes are distinctly different and are also different from that for the $PtAu_8^{2+}$ complex (Figure 2), especially within the lower energy region (below 2.5 μm^{-1}). On the other hand, the MCD spectra in this same region for the $Pt(HgX)_2Au_8^{2+}$ complexes are similar to the MCD spectrum of the $Pt(CO)Au_8^{2+}$ complex (Figure 3). Within the region of ∼2.5−3.3 μm^{-1}, the MCD spectrum for the $Pt(Hg)_2Au_8^{2+}$ complex exhibits some features analogous to those corresponding to bands III−V in the $PtAu_8^{2+}$ MCD spectrum. The pattern of the MCD spectra for the $Pt(HgX)_2Au_8^{2+}$ complexes also compares favorably within this same region (∼2.5−3.3 μm^{-1}) yet is uniformly negative.

A schematic HMO energy level diagram for the $Pt(Hg)_2Au_8^{2+}$, $Pt(Hg)_2Au_8^{4+}$ (which serves as a model for $Pt(HgNO_3)_2Au_8^{2+}$), and $Pt(HgCl)_2Au_8^{2+}$ cluster complexes was developed by using the diagram for $PtAu_8^{2+}$ as a starting point and adding energy levels for the two Hg^0, Hg^I, or $ClHg^I-$ ligands.[22] The schematic diagram is given in Figure 9. The additional excited configurations involving the $2a_1$ and $1b_2$ Hg-based orbitals which give allowed excited states are found in Table 3. The MCD spectra for the $Pt(Hg)_2Au_8^{2+}$ and the $Pt(HgX)_2Au_8^{2+}$ complexes can exhibit both *A* and *B* terms, the signs of which were determined by means of eqs 1−3 by using the same procedure for $PtAu_8^{2+}$.

The broad features in the electronic absorption and MCD spectra reflect the large number of states and are likely to include a number of unresolved transitions in each case. Nevertheless a qualitative interpretation is presented. Just as the addition of CO to the $PtAu_8^{2+}$ complex affected the lower energy region of the MCD spectrum ascribed to Pt → Au transitions, the addition of Hg(0) and XHg− ligands to the $PtAu_8^{2+}$ complex seems to have a similar affect. This is not surprising because the platinum 5d orbitals are accessible to the Hg or XHg− ligands along the *z*-axis. In D_{4d} symmetry, the empty mercury p_x and p_y orbital π combinations have e_3 symmetry and can overlap with the filled Pt 5d π orbitals of the same symmetry. While the Hg(0) and XHg− ligands donate electron density

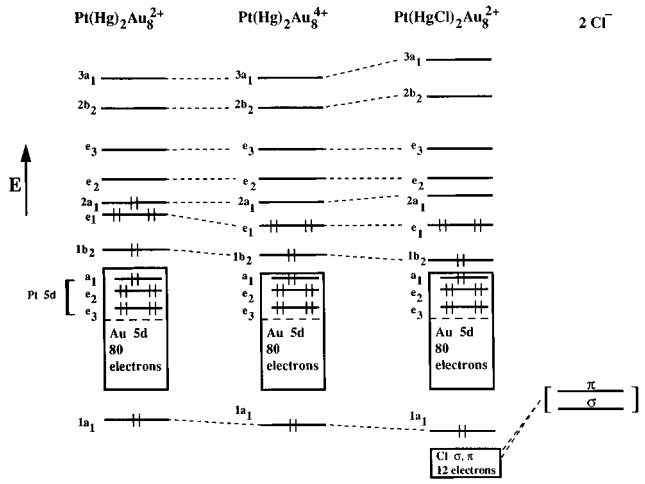

Figure 9. Schematic molecular orbital energy levels for $Pt(Hg)_2Au_8^{2+}$ (left), $Pt(Hg)_2Au_8^{4+}$ (center), and $Pt(HgCl)_2Au_8^{2+}$ (right), assuming D_{4d} symmetry.

through their σ s or sp hybrid orbitals, respectively, they also may be visualized as accepting π electron density into their empty p orbitals from the filled Pt 5d orbitals in much the same way as CO. Both the absorption and MCD spectra for $Pt(Hg)_2Au_8^{2+}$ and the $Pt(HgX)_2Au_8^{2+}$ complexes show no features below energies ∼2.0 μm^{-1}. Therefore transitions to excited states for $PtAu_8^{2+}$ observed in this region must be blue-shifted for the $Pt(Hg)_2Au_8^{2+}$ and $Pt(HgX)_2Au_8^{2+}$ complexes. One reasonable explanation for the blue-shift of the low-energy IF Au_8^{2+} transitions is that the HOMO e_1 level is stabilized by the empty Hg ligand p_x and p_y orbitals. Furthermore, the MCD spectra for the $Pt(HgX)_2Au_8^{2+}$ complexes show that the Pt 5d π orbitals must be stabilized also because the Pt → Au transitions believed responsible for the MCD for the $PtAu_8^{2+}$ complex are absent in this lower energy region.

$Pt(Hg)_2Au_8^{2+}$ Spectra. For the $Pt(Hg)_2Au_8^{2+}$ complex, the broad nature of bands I−III, Figure 5, and multiple features of the MCD spectrum imply several additional excited states to those already assigned for the $PtAu_8^{2+}$ complex in the lower energy region. Some reasonable possibilities for these excited states are given in Table 3 and involve the Hg-based MO's $2a_1$ and $1b_2$, for example, the $15E_1(^3E_2)$, $11E_3(^3E_2)$, $18E_1(^3E_2)$, and $15E_3(^3E_2)$ states of triplet origin, each having predicted negative MCD *A* terms, which could be visualized as adding to the positive MCD *A* term features that result from the Pt → Au transitions or the IF Au_8^{2+} transitions and thus give rise to the observed complicated MCD spectrum. The broadness of band III for the $Pt(Hg)_2Au_8^{2+}$ complex, along with the negative and positive MCD features at 2.56 and 2.72 μm^{-1}, respectively, which resemble a positive *A* term, may signal the presence of the transitions to the $12E_3(^1E_3)$ and $13E_3(^3E_3)$ states, both of which predict positive MCD *A* terms.

At energies > ∼2.7 μm^{-1}, Figure 5, the pattern in the MCD spectrum for $Pt(Hg)_2Au_8^{2+}$ complex is similar to that observed for the $PtAu_8^{2+}$ complex (Figure 2). For example, the MCD features at 2.72 (pos), 2.92 (neg), and 3.10 (neg) μm^{-1}, respectively, for the $Pt(Hg)_2Au_8^{2+}$ complex present a similar shape to the negative MCD features at 2.59, 2.71, and 2.84 μm^{-1} for the $PtAu_8^{2+}$ complex, even though the MCD feature at 2.59 μm^{-1} remains negative. These similarities argue for the same type of transitions in the spectra for the $Pt(Hg)_2Au_8^{2+}$ complex. The IF Au_8^{2+} assignments made for the $PtAu_8^{2+}$ complex in the region of ∼2.5−3.1 μm^{-1} are also reasonable for the $Pt(Hg)_2Au_8^{2+}$ complex in the region of ∼2.6−3.3 μm^{-1}. The appearance of the broad, poorly resolved absorption bands IV and V in the region of ∼2.7−3.4 μm^{-1} for $Pt(Hg)_2Au_8^{2+}$

complex is consistent with the states having slightly higher energies and being closer together compared to the $PtAu_8^{2+}$ complex.

Due to the broad nature of band VI, Figure 5, with a large intensity and the large negative feature in the MCD spectrum for the $Pt(Hg)_2Au_8^{2+}$ complex, several excited states must be present. Band VI is logically assigned to the same transitions assigned for bands V−VII of the $PtAu_8^{2+}$ complex (Figure 2). This seems reasonable because the negative MCD features for bands V and VI of the $PtAu_8^{2+}$ complex, if shifted slightly to higher energy, could be visualized to add to the negative MCD feature for band VII resulting in the large negative MCD feature observed for the $Pt(Hg)_2Au_8^{2+}$ complex. Other transitions, for example, to the $9B_2(^1B_2)$, $16E_1(^3B_2)$, $19E_1(^1E_1)$, $20E_1(^3E_1)$, and $11B_2(^3E_1)$ states may also be in this region and contribute to the large absorption intensity as well as the large negative MCD feature. This interpretation is admittedly speculative but seems reasonable on the basis of the energy level scheme in Figure 9.

$Pt(HgX)_2Au_8^{2+}$ (X = Cl^-, NO_3^-) Spectra. For the $Pt(HgX)_2Au_8^{2+}$ complexes, the shape of the MCD spectrum at energies $< \sim 2.5\ \mu m^{-1}$, Figure 6, is similar to that of the $Pt(CO)Au_8^{2+}$ complex, Figure 3, and is also similar to that of the $PdAu_8^{2+}$ complex, Figure 1. Thus the lower energy region of the spectra for the $Pt(HgX)_2Au_8^{2+}$ complexes should be assigned to the same IF Au_8^{2+} transitions that were assigned for the $PdAu_8^{2+}$ and $Pt(CO)Au_8^{2+}$ complexes. Bands I and II for the $Pt(HgX)_2Au_8^{2+}$ complexes are therefore assigned to the IF Au_8^{2+} transitions to the $2E_3(^3E_3)$, $1E_3(^1E_3)$, $2E_1(^3E_1)$, and $1E_1(^1E_1)$ states. The transitions to the $14E_1(^3E_1)$ and $13E_1(^1E_1)$ states, predicted to have negative *A* terms, from the lowest energy configuration $e_1^3 2a_1$ must also be in this lower energy region.

Unlike the higher energy region ($> \sim 2.5\ \mu m^{-1}$) in the MCD spectrum for the $Pt(Hg)_2Au_8^{2+}$ complex, the MCD spectrum in this same region for the $Pt(HgX)_2Au_8^{2+}$ complexes, Figure 6 and Table 1, is less similar to that of the $PtAu_8^{2+}$ complex (Figure 2). With the blue-shift of both the IF Au_8^{2+} transitions and the Pt → Au transitions, combined with additional transitions from the filled $1b_2$ MO level, it is easy to see why the MCD spectrum should not be similar. Bands III and IV for the $Pt(HgX)_2Au_8^{2+}$ complexes are assigned to the IF transitions to the $4E_1(^3B_2)$ and $5E_1(^3E_2)$ states, assigned to the energy region of bands III and IV for the $PtAu_8^{2+}$ complex. Other transitions are likely present to account for the broadness in the absorption bands and their corresponding obscure MCD features, for example, the transitions to the $17E_1(^3B_2)$, $18E_1(^3E_1)$, and $15E_3(^3E_3)$ states, predicted to have negative MCD *A* terms, which would give rise to a complicated MCD spectrum in the region of bands III and IV.

Because the same energy absorption band and the corresponding MCD feature at $\sim 2.83\ \mu m^{-1}$ are seen for both the $PtAu_8^{2+}$ and $Pt(HgX)_2Au_8^{2+}$ complexes, band V for the $Pt(HgCl)_2Au_8^{2+}$ complex, which is unresolved in the broad absorption for $Pt(HgNO_3)_2Au_8^{2+}$, is logically assigned to the IF Au_8^{2+} transition to the $3B_2(^1B_2)$ state, identical to the assignment made for band IV for the $PtAu_8^{2+}$ complex. Band VI is assigned to the transition to $6E_1(^1E_1)$ by analogy to band VI for $PtAu_8^{2+}$. The Pt → Au transitions to the $11E_1(^1E_1)$, $12E_1(^3E_1)$, $9E_3(^1E_3)$, and $10E_3(^3E_3)$ states and the IF Au_8^{2+} transitions to the $19E_1(^1E_1)$, $20E_1(^3E_1)$, and $11B_2(^3E_1)$ states may also be present in this energy region and account for the unresolved, complex negative MCD spectrum for the $Pt(HgX)_2Au_8^{2+}$ complex.

Even though there are similarities between the spectra for the $PtAu_8^{2+}$, $Pt(Hg)_2Au_8^{2+}$, and $Pt(HgX)_2Au_8^{2+}$ complexes, spectral congestion is evident for the Hg(0) and XHg− complexes. The large number of allowed excited states contributes to unresolved transitions. This makes *detailed* assignments difficult, yet the broad qualitative interpretation presented seems reasonable and plausible. Greater precision in locating transitions to individual states will require more resolved spectra, perhaps from low-temperature absorption and MCD measurements.

Concluding Remarks

The MO schemes in Figures 7 and 8 can be used to interpret the absorption and MCD spectra for $PdAu_8^{2+}$ and $PtAu_8^{2+}$ in a reasonable and internally consistent way. It must be acknowledged, however, that the detailed assignments proposed here may not be unique because of the numerous states (Table 3) which are possible based on the relatively simple model for skeletal MO's constructed from Pd 5s and Pt and Au 6s valence orbitals. Nevertheless, and even though the absorption and MCD spectra for $PdAu_8^{2+}$ and $PtAu_8^{2+}$are complicated, similarities are seen when these spectra are compared, and when they are compared to the spectra for Au_9^{3+}, with the help of the correlation in Figure 8. These similarities, together with the predicted MCD term signs, guide the assignments to give an internally consistent model based on the same type of IF transitions for all three cluster complexes. Furthermore, the striking low-energy MCD spectral changes observed on the substitution of the Pt atom for Pd or Au are interpreted as due to the presence of Pt 5d → Au 6s transitions. The Pt 5d → Au 6s transitions are proposed because of the higher energy of the Pt 5d orbitals in comparison to the Au 5d orbitals in the $PtAu_8^{2+}$, which place them among the highest energy occupied MO's of the cluster complex. The MCD *A* terms for these transitions are expected to be stronger and are envisioned as overlapping and dominating the weaker IF MCD features anticipated in this region. Changing the Au-bound phosphine ligand from PPh_3 to P(*p*-tolyl)$_3$ or bonding $AgNO_3$ or CuCl to the side of the Au skeletal structure causes little change in the MCD spectral pattern. However when CO, Hg(0), or XHg− ligands are bonded to the center Pt, the MCD is greatly changed in the low-energy region. These observations are fully consistent with the presence of the Pt 5d orbitals among the highest energy occupied MO's of the cluster complex. The Pt 5d orbital involvement and the Pt → Au transitions proposed in the lower energy region of the spectra are expressed in different ways for each complex. The $Pt(Hg)_2Au_8^{2+}$ cluster complex, on the one hand, has an MCD spectrum in the lower energy region showing similarities to the MCD spectrum for the $PtAu_8^{2+}$ complex. This points toward the Pt 5d orbitals being involved in Pt−Hg bonding to only a small degree and, therefore, is consistent with the experimental finding that the complex reversibly dissociates Hg atoms to give $Pt(Hg)Au_8^{2+}$ or $PtAu_8^{2+}$.[16] On the other hand, the lower energy region of the MCD spectra for the $Pt(HgCl)_2Au_8^{2+}$ or $Pt(HgNO_3)_2Au_8^{2+}$complexes and $Pt(CO)Au_8^{2+}$-complex is very similar, and in these cases the spectra are interpreted in terms of a shift of the Pt → Au transitions to higher energy. In these complexes the bonding of the XHg− and CO ligands to $PtAu_8^{2+}$ is strong and irreversible.[9b,16] The Pt 5d orbitals must be involved in ligand binding to a greater extent in $Pt(CO)Au_8^{2+}$ and $Pt(HgX)_2Au_8^{2+}$ than in $Pt(Hg)_2Au_8^{2+}$. The Pt−HgCl stability is also borne out by experimental results which show the complex's ability to retain the ClHg− ligands when a PPh_3 is displaced by Cl^-.[17] The presence of the Pt 5d orbitals among the highest occupied MO's in the cluster complex may be partly responsible for the greater reactivity of $PtAu_8^{2+}$ with electrophilic ligands such as H_2 (or D_2), CO, RNC, Hg(0), and XHg− compared to $PdAu_8^{2+}$ or Au_9^{3+}.

Acknowledgment. The authors thank Professor Louis H. Pignolet for providing samples of the Pt-centered cluster complexes and for helpful discussions.

IC9606993